Numerical studies on impurity transport in the W7-AS island divertor

Y. Feng, F. Sardei, J. Kisslinger, D. Reiter[1], Y. Igitkhanov
Max-Planck-Institut für Plasmaphysik, EURATOM-Association, D-85748 Garching, Germany
[1]Institut für Plasmaphysik, Forschungszentrum Jülich Gmbh, EURATOM Association, Trilateral Euregio Cluster, D-52425 Jülich, Germany

1. Introduction

Basic features of the island divertor concept have been investigated theoretically and experimentally in the past few years [1-4]. A realistic plasma transport modelling for these configurations has become possible by the development of the EMC3-EIRENE code [5,6], which was already applied successfully to W7-AS [7,8]. Recently the code has been extended to impurity transport, which now allows a self-consistent treatment of plasma, neutrals and impurities taking into account the complex 3D island structures and the discontinuous divertor plates and baffles.

2. Impurity model

As a first step, a simplified impurity transport model has been implemented in the EMC3-EIRENE code:
Continuity:

$$\nabla\cdot\left(n_I V_{I//}\boldsymbol{b} - D_I \boldsymbol{b}_\perp \boldsymbol{b}_\perp\cdot\nabla n_I\right) = -S_{z\to z+1} - R_{z\to z-1} + S_{z-1\to z} + R_{z+1\to z} \qquad (1)$$

Momentum (force balance):

$$U_{Ii}\left(V_{I//} - V_{i//}\right) = -\boldsymbol{b}\cdot\nabla n_I T_I + n_I e Z_I \boldsymbol{E}_{//} + n_I Z_I^2 C_e \boldsymbol{b}\cdot\nabla \boldsymbol{T_e} + n_I C_i \boldsymbol{b}\cdot\nabla \boldsymbol{T_i} \qquad (2)$$

$$n_e e\boldsymbol{E}_{//} + \boldsymbol{b}\cdot\nabla n_e T_e + n_e C_e \boldsymbol{b}\cdot\nabla \boldsymbol{T_e} = 0 \qquad (3)$$

with $T_I = T_i$. The model applies to light impurities at small concentrations, $Z_I^2 n_I << n_e$, which excludes contributions of impurities to the plasma transport equations other than by radiation losses. High density and low temperature are assumed in the momentum equation. In the present study carbon released from the target by sputtering processes is assumed to be the only impurity species.

An example of how the discontinuous target plates affect the distribution of the lower ionisation states of carbon over an island tube cut by the plates and baffles is shown in Fig. 1. The power entering the SOL is P_{SOL}=1MW, the upstream plasma density at the separatrix n_u = 8x10^{13} cm^{-3}, the total carbon sputtering coefficient S_c= 0.5, which is small enough to keep the radiation zone attached to the plates at $T_e \approx 8\,eV$. The first ionisation

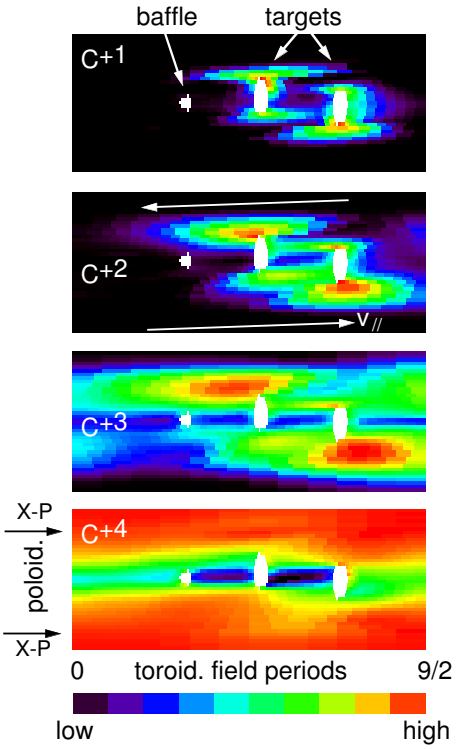

Fig. 1: Strong helical modulation of low carbon ionisation states along an island tube intersecting the targets

state is strongly localised near the plates due to its short life time. The higher states live longer, spread in toroidal and poloidal direction and get shifted downstream by friction with the main plasma flow. C^{4+} is homogeneous everywhere except in the shadowed regions between the plates, higher ionisation states are not present at the given SOL temperatures.

3. Detachment

3.1 Modelling results

In order to explore the detachment physics in the W7-AS island divertor, a dedicated transport study including intrinsic carbon impurities was carried out with the EMC3-EIRENE code. The impurity concentration C was controlled by the sputtering coefficient S_c, which was varied as a free parameter from 0.5% to 5% (Fig. 2). A total power of 1 MW entering the island SOL was kept fixed in all simulations, the transport coefficients were D=0.5 m^2/s for both hydrogen and carbon, and $\chi_e = \chi_i = 3D$. Three upstream plasma density values were used, n_u= 4x10^{13}, 6x10^{13} and 8x10^{13} cm^{-3}. In the lowest density case, the carbon radiation increases smoothly from 5% to 40%, reflecting essentially the linear

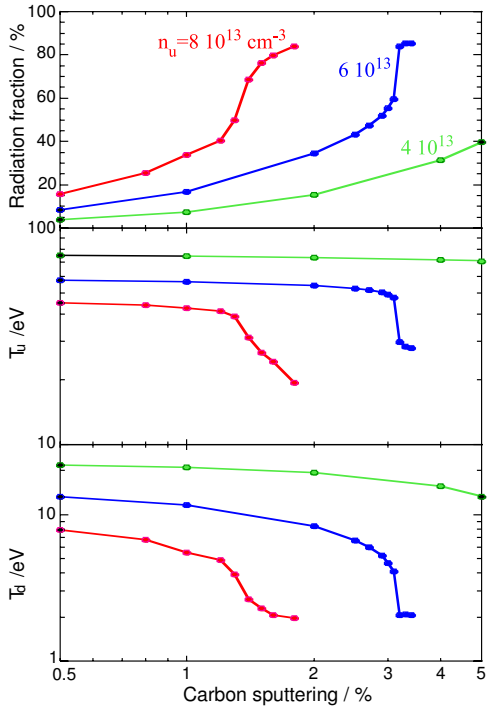

Fig. 2: Sharp increase of radiation and drop of T at detachment transition

scaling of the radiation with the impurity density. The up- and downstream temperatures are almost insensitive to S_c, indicating a weak impact of the radiation on the power balance in the SOL. For the intermediate density, n_u= 6x10^{13} cm^{-3}, the carbon radiation first increases smoothly with S_c up to 3.1% and then jumps to a high radiation level at which the carbon radiates more than 80% of the SOL input power. The jump is accompanied by a sharp drop of both the up- and downstream temperatures. A concomitant drop of the pressure and recycling flux (not shown in the picture) indicates detachment. If n_u is increased to 8x10^{13} cm^{-3}, the value of S_c needed for detachment is shifted down to 1.5% and the detachment transition becomes smoother. In all cases the contribution from hydrogen radiation to the power balance stays below 10%. The radiation zone is thin (≈1 cm) compared to the island size (≈5 cm) and jumps from the target to the X-point at detachment transition. The target power load drops strongly at detachment and hot spots disappear, indicating a broad deposition profile.

Both effects, the sharp raise of the radiation level and the jump of the radiation zone, could be reproduced, for the same input parameters and transport coefficients, by a 1D radial energy transport model taking into account only diffusive heat transport and boundary conditions given by the upstream and downstream heat fluxes. This confirms the predominant role of the cross-field transport in the W7-AS island divertor resulting from the very small pitch of the field lines typical for island divertors and the small size of the W7-AS divertor islands [7].

3.2 Detachment condition

Integrating the radial power balance with impurity radiation loss term

$$dq/dx = -Cn^2 L(T) \tag{4}$$

between the up- and downstream positions and assuming a predominant cross-field heat flux $q = -\chi n\, dT/dx$, one obtains

$$q_u^2 - q_d^2 = \int_{T_d}^{T_u} 2C\chi n^3 L(T)dT \tag{5}$$

with $q_u = P_{SOL}/4\pi^2 Ra$, $q_d = \Theta n c_s(\gamma T_d + 31eV)$, $c_s = \sqrt{2T_d/m_i}$, Θ = field line pitch.
In a detached state $T_d \to 0$ and eq. (5) reduces to

$$q_u = \sqrt{\int_0^{T_u} 2C\chi n^3 L(T)dT}\,. \tag{6}$$

For a thin radiation layer compared to the gradient length of $C\chi n^3$, the RHS of eq. (6) becomes

$$\sqrt{\int_0^{T_u} 2C\chi n^3 L(T)dT} \approx \sqrt{\underbrace{\int_0^{\infty} L(T)dT}_{const}} \sqrt{(2C\chi n^3)_{x_{rad}}} \tag{7}$$

with $const\sqrt{(2C\chi n^3)_{x_{rad}}}$ being the radiation capability profile at x_{rad}, the location of the radiation layer. Detachment occurs if the radiation capability at the target equals or exceeds the input power:

$$const\sqrt{(2C\chi n^3)_{x_{target}}} \geq q_u \tag{8}$$

The detachment is stable within the SOL if the radiation capability is higher than the input power at the target and lower at the upstream SOL position:

$$const\sqrt{(C\chi n^3)_{x_{target}}} > q_u > const\sqrt{(C\chi n^3)_{x_u}} \tag{9}$$

3.3. Bifurcation and thermal instability

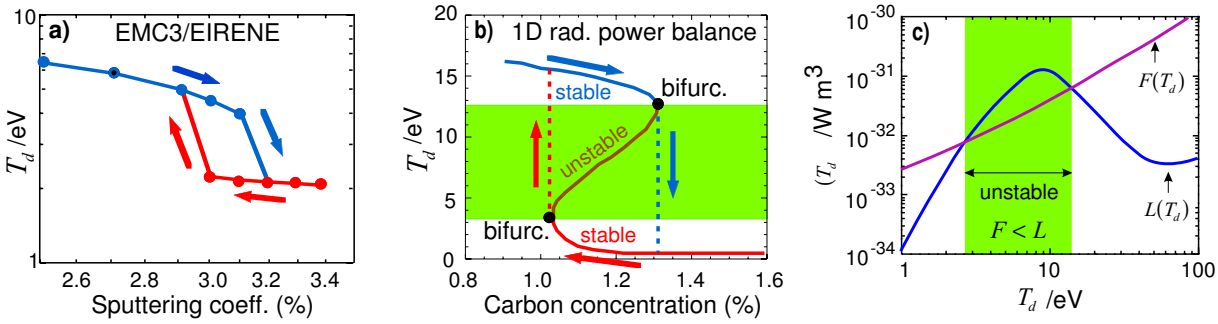

Fig. 3: Two-branch transition (hysteresis loop) between attached and detached state

A refined numerical S_c scan with EMC3-EIRENE in the range of detachment transition shows that the forward and backward transitions occur at different values of S_c giving rise to a hysteresis loop (Fig. 3a). This effect is related to the form of the cooling rate function $L(T)$ (Fig. 3c) and becomes obvious by inspecting the radial power balance, eq. (5). This equation has three solutions branches for T_d (C) in a small range of impurity concentrations C, namely two stable branches, corresponding to the high and low T_d legs of $L(T)$, and an unstable intermediate branch connecting the two (Fig. 3b). The three branches can be easily identified by taking the derivative of T_d with respect to C from eq. (5) for a fixed input power q_u:

$$\frac{\partial T_d}{\partial C} = \frac{\frac{1}{C}\int_{T_d}^{T_u} L(T)dT}{L(T_d) - F(T_d)} \tag{10}$$

with

$$F(T_d) = const\frac{2\Theta^2}{m_i}\left(\frac{n}{q_u}\right)^2 (3\gamma T_d + 31eV)(\gamma T_d + 31eV). \tag{11}$$

The two solution branches are characterised by the sign of $\partial T_d/\partial C$, i.e. by the relative magnitude of $L(T_d)$ and $F(T_d)$:

$$\begin{array}{lll} F(T_d) > L(T_d) \;\Rightarrow\; \partial T_d/\partial C < 0 & \text{stable high and low solutions,} & \\ F(T_d) = L(T_d) \;\Rightarrow\; \partial T_d/\partial C = \infty & \text{bifurcation,} & (12) \\ F(T_d) < L(T_d) \;\Rightarrow\; \partial T_d/\partial C > 0 & \text{unstable solution.} & \end{array}$$

The unstable branch is not accessible. If C is increased beyond the high-T_d bifurcation point, the plasma enters the unstable T_d domain and relaxes into the stable low-T_d solution. The reverse transition occurs if C is decreased beyond the low-T_d bifurcation point. For given q_u, the $F(T_d)$ function scales as n^2, i.e. by increasing n the unstable T_d domain and hence the hysteresis loop shrink and eventually disappear. This explains why the sharp transition to detachment becomes smoother at the highest density case shown in Fig. 2.

References

[1] J. Kisslinger et al., 21st EPS, Montpellier 1994, Europhys. Conf. Abstracts 18B, part I, 368
[2] F. Sardei et al., J. Nucl. Mat. 241-243 (1997) 135
[3] P. Grigull et al., J. Nucl. Mat. 241-243 (1997) 935
[4] A. Komori, N. Ohyabu et al., Proc. 16th Int. Conf. on Fusion Energy, Montreal 1996, IAEA, Vienna 1997, Vol.2, 3
[5] Y. Feng, F. Sardei, J. Kisslinger, J. Nucl. Mat. 266-269 (1999) 812
[6] D. Reiter, Technical Report Jül-1947, KFA Jülich, Germany, 1984
[7] Y. Feng, J. Kisslinger, F. Sardei, 26th EPS Conf., Maastricht 1999
[8] Y. Feng et al., Plasma Phys. Contr. Fusion 40 (1998) 371